DMD Fast Forward. Published on March 24, 2011 as doi:10.1124/dmd.110.037820

DMD# 37820

DISPOSITION AND DRUG-DRUG INTERACTION POTENTIAL OF VELIPARIB (ABT-888), A NOVEL AND POTENT INHIBITOR OF POLY(ADP-RIBOSE) POLYMERASE

Xiaofeng Li, Juergen Delzer, Richard Voorman, Sonia M. de Morais, and Yanbin Lao

Drug Metabolism, Pharmacokinetics and Bioanalysis, Abbott Laboratories, Abbott Park, Illinois (X. L., R. V., S. M. de M., Y. L.); Ludwigshafen, Germany (J. D.)

DMD# 37820

Running title: Disposition and Drug-Drug Interaction Potential of Veliparib

Corresponding author: Yanbin Lao

Drug Metabolism, Pharmacokinetics and Bioanalysis, Abbott Laboratories, Abbott Park, IL 60044

Tel: 847-938-6604

Fax : 847-937-8330

Email: Yanbin.Lao@abbott.com

Text Pages : 28

Tables : 3

Figures : 4

References : 21

Abstract : 244

Introduction : 630

Discussion : 1496

Abbreviations: amu: atomic mass units; AUC, area under the curve; BBB, blood-brain barrier; BCRP, breast cancer resistance protein; B:P, brain-to-plasma ratio; CID, collision-induced dissociation; DDI, drug-drug interaction; HPLC-MS/MS, high performance liquid chromatography tandem mass spectrometry; LSC, liquid scintillation counting; MS, mass spectrometry; PARP, poly (ADP-ribose) polymerase; P-gp, p-glycoprotein; TMZ, temozolomide.

ABSTRACT

The disposition of veliparib, ((*R*)-2-(2-methylpyrrolidin-2-yl)-1*H*-benzo[*d*]imidazole-4-carboxamide, ABT-888), a novel and potent inhibitor of poly(ADP-ribose) polymerase for the treatment of cancers, was investigated in rats and dogs after intravenous and oral administration of [^{3}H]veliparib, and compared to humans. Veliparib absorption was high. Dosed radioactivity was widely distributed in rat tissues. The majority of drug-related materials was excreted in urine as unchanged drug (approximately 54, 41 and 70 % of the dose in rats, dogs and humans, respectively). A lactam M8 and an amino acid M3 were two major excretory metabolites in animals. In the circulation of animals and humans, veliparib was the major drug-related component and M8 was one of the major metabolites. Mono-oxygenated metabolite M2 was significant in the rat and dog, and M3 was also significant in the dog. Veliparib biotransformation occurred on the pyrrolidine moiety *via* formation of a lactam, an amino acid and an *N*-carbamoyl glucuronide, in addition to oxidation on benzoimidazole carboxamide and sequential glucuronidation. *In vitro* experiments using recombinant human cytochrome P450 enzymes (CYPs) identified CYP2D6 as the major enzyme metabolizing veliparib with minor contributions from CYP1A2, 2C19 and 3A4. Veliparib did not inhibit or induce the activities of major human CYPs. Veliparib was a weak P-glycoprotein (P-gp) substrate, showing no P-gp inhibition. Altogether, these studies indicate a low potential for veliparib to cause clinically significant P-gp or CYP –mediated drug-drug interactions (DDIs). Overall, the favorable dispositional and DDI profiles of veliparib should be beneficial to its safety and efficacy.

INTRODUCTION

Cancer is the second leading cause of death in the US, contributing to 23.2% of all deaths (562,875 deaths) in 2007 (Xu et al., 2010). It is estimated that 1,529,560 new cases of cancer will be diagnosed and 569,490 Americans will die of cancer in 2010 (American Cancer Society, 2010). An increased knowledge about the disease and its causes has resulted in identification of numerous new targets for potential anti-cancer therapies. Inhibition of poly(ADP-ribose) polymerase (PARP) has been shown to be a promising novel mechanism through targeting DNA repair. PARPs are a family of 17 enzymes that catalyze the transfer of ADP-ribose units to acceptor proteins to form ADP-ribose polymer, which is involved in multiple cellular processes such as replication, transcription and differentiation. PARP-1 is activated by DNA damage and is primarily responsible for initiating the repair of single-strand DNA break *via* a base excision repair (BER) pathway. When co-administrated with DNA-damaging chemotherapeutics, PARP inhibitors could potentiate the efficacy of these agents by preventing the repair of the damaged DNA through BER (Rouleau et al., 2010; Papeo et al., 2009). Thus, PARP inhibitors could be developed as chemosensitizers of DNA-damaging agents. PARP inhibitors have also demonstrated single agent effects in selected genetic backgrounds such as tumors with defects in the breast cancer associated genes (*BRCA*-1 and -2), the homologous recombination (HR) DNA repair regulators. PARP inhibition blocks BER pathway and results in “synthetic lethality” effects towards HR-deficient tumors (Rouleau et al., 2010; Papeo et al., 2009).

In addition to veliparib, several other PARP inhibitors are currently in various stages of clinical development, including iniparib, olaparib, PF-1367338, MK-4827, and

CEP-9722. These agents are being developed as chemopotentiators of DNA-damaging chemotherapeutics for treatment of solid tumors (e.g. melanoma and glioma), and as single agents in BRCA-deficient breast or ovarian cancers. Efficacy and safety data from Phase I and II trials demonstrated that PARP inhibitors in combination of cytotoxic agents were well tolerated and showed anti-tumor activity (Penning, 2010).

Veliparib ((*R*)-2-(2-methylpyrrolidin-2-yl)-1*H*-benzo[*d*]imidazole-4-carboxamide, Figure 1) is a novel and potent inhibitor of PARP-1 and PARP-2 enzymes (Ki's of 5 and 2 nM, respectively) and has demonstrated excellent *in vivo* efficacy in a broad spectrum of preclinical tumor models in combination with a variety of cytotoxic agents such as temozolomide (TMZ), cisplatin, cyclophosphamide and radiation (Donawho et al., 2007; Palma et al., 2009; Penning et al., 2009). Preclinical pharmacokinetic profiles of veliparib were characterized by high plasma clearance, high volumes of distribution, and high oral bioavailability across species (Donawho et al., 2007). A Phase 0 clinical study of veliparib showed the statistically significant inhibition of PARP activity in tumor biopsies and peripheral blood mononuclear cells at a single oral dose of 25 or 50 mg (Kummar et al., 2009). The preliminary human pharmacokinetic profile was characterized by rapid absorption (T_{max}: 0.5-1.5 h postdose) and primary urinary excretion (on average, 70% of dose in urine as unchanged parent drug at the 50-mg dose) (Kummar et al., 2009). In patients receiving veliparib, the lactam metabolite M8 was shown to be a major human plasma metabolite (Wiegand et al., 2010). Preliminary Phase I study results for veliparib in combination of TMZ in patients with solid tumors indicated that the treatment was well tolerated and demonstrated anti-tumor activity (Molina et al., 2009). Currently, veliparib is being investigated in multiple clinical trials

for human cancers either in combination with cytotoxic agents or as a monotherapy (clinicaltrials.gov).

The objectives of the current study were as follows: 1) to characterize disposition of veliparib in rats and dogs, two animal species used for safety assessment; 2) to elucidate the structures of veliparib metabolites; 3) to characterize the interactions of veliparib with human P-glycoprotein (P-gp) and assess P-gp-mediated drug-drug interactions (DDIs); 4) to conduct *in vitro* assessment of DDIs mediated by cytochrome P450 enzymes (CYPs).

DMD Fast Forward. Published on March 24, 2011 as DOI: 10.1124/dmd.110.037820
This article has not been copyedited and formatted. The final version may differ from this version.

MATERIALS AND METHODS

Materials

Veliparib and its lactam metabolite (M8) were synthesized, as described previously (Penning et al., 2009). [^{3}H]Veliparib was synthesized by Radiochemistry Group, Process Research and Development, Abbott Laboratories. The specific activity of [^{3}H]veliparib was 3.2 Ci/mmol and radioactivity purity was greater than 99 %. All chemicals were of analytical grade and purchased from Sigma-Aldrich (St. Louis, MO). Chromatography-grade solvents were supplied by EMD (Gibbstown, NJ) or Sigma-Aldrich. Supersomes were purchased from BD Gentest (Woburn, MA).

Animal Studies

Animal studies were conducted in accordance with the guidance established by the Abbott Institutional Animal Care and Use Committees. [^{3}H]Veliparib and non-radiolabeled veliparib were dissolved in a mixture of ethanol and 5 % dextrose in water (10/90, v/v) to make a dosing solution at a final concentration of 5 mg/ml. The dose volume was 1.0 ml/kg for rats and 0.5 ml/kg for dogs for both intraveneous and oral dosing. The dosed radioactivity was approximately 160 μCi/rat and 340 μCi/dog. Pre- and post-dosing radioactivity purities of the dose solutions were greater than 99 %.

Dosing of [^{3}H]Veliparib to Rats

Male Sprague-Dawley rats (220-300 g), age 8-12 weeks, were used in the studies. For bile collection, six surgically-modified animals with cannulas inserted into both bile duct and duodenum (Hilltop Lab Animals, Inc, Scottsdale, PA) were acclimated for

approximately four days prior to dose administration. The rats were housed individually in metabolism cages and fasted overnight prior to dosing. Food was provided 4 hours after dosing. On the day of dosing, the biliary and duodenal cannulas were disconnected and a solution of taurocholic acid (27.8 mg/ml) was infused through the duodenal cannula. Groups of three rats each received a single 5 mg/kg intravenous dose of [^{3}H]veliparib *via* the superficial penile vein or a 5 mg/kg oral dose of [^{3}H]veliparib. Isoflurane was used as anesthesia during the procedure. Bile, urine, and feces were collected at the following collection intervals: 0-6, 6-24, 24-48, 48-72 h for bile and 0-24, 24-48, 48-72 h for urine and feces. The cages were washed at the end of study with a small amount of 70 % ethanol in water and the cage wash was collected for determination of total radioactivity. To obtain plasma samples for metabolite identification and profiling, a group of three surgically-modified rats with femoral artery cannulas from Hilltop Lab Animals, Inc was given a single 5 mg/kg intravenous dose of [^{3}H]veliparib *via* the superficial penile vein. Serial blood samples (0.5 ml at each time point) were taken *via* Culex automated blood sampling system (BASi, West Lafayette, IN) from individual rat at 0.5, 1, 2, 4, 6 and 24 h postdose. Blood samples were centrifuged at 3000 rpm at 4ºC to separate plasma (Jouan CR3 centrifuge, rotor model T40, Thermo Fischer Scientific, Waltham, MA), which were stored at -20ºC until analysis.

To investigate tissue distribution of [^{3}H]veliparib, fourteen rats were given a 5 mg/kg intravenous dose of [^{3}H]veliparib *via* the superficial penile vein. Subgroups of two rats were euthanized at 0.5, 1, 2, 4, 6, 24 and 48 h for collection of blood and selected tissues (bone, bone marrow, brain, eye, heart, kidney, liver, lung, muscle, skin, spleen, spinal cord, testes, thymus, white fat). Blood samples were withdrawn *via* cardiac

puncture into heparinized tubes using Vacutainers™ (BD, Franklin Lakes, NJ). Plasma samples were separated from blood by centrifugation.

Dosing of [^{3}H]Veliparib to Dogs

Two male beagle dogs (10-11 kg), age 2-2.5 years, were obtained from Marshall Research Animals (North Rose, NY), and surgically prepared at Abbott with cannulas inserted into the bile duct and duodenum. One single dog received a 2.5 mg/kg intravenous or oral dose of [^{3}H]veliparib. Bile, urine, and feces were collected at the same intervals as those in rats. The cages were washed daily and the cage wash was collected for determination of total radioactivity. Serial blood samples (5 ml at each time point) were taken from individual dog at 0.25, 0.5, 1, 2, 3, 4, 6, 8, 24 and 48 h postdose. Blood samples were centrifuged to separate plasma which were then stored at -20ºC until analysis.

***In Vitro* Incubations with Recombinant Human CYPs (Supersomes)**

The *in vitro* metabolism of [^{3}H]veliparib was investigated with a panel of recombinant human CYP isoforms, including CYP1A1, CYP1A2, 2A6, 2B6 , 2C8, 2C9*1, 2C18, 2C19, 2D6*1, 3A4, 3A5, and 2E1. An incubation mixture (150 µl) contained individual protein (100 pmol/ml) and [^{3}H]veliparib (0.5 µM) in 50 mM potassium phosphate buffer at pH 7.4. The reaction was initiated by addition of 1 mM NADPH and incubated at 37^{o}C for 60 min. Reaction was terminated by addition of 1 volume solution of acetonitrile/methanol (50/50, v/v). After vortexing and centrifugation, the supernatant was analyzed by HPLC analysis with radioactivity detection. To identify metabolites, [^{3}H]veliparib (10 µM) was incubated with CYP1A1, 2C19, 2D6*1 or 3A4

(100 pmol/ml) at 37°C for 60 min. The processed samples were analyzed by HPLC-MS/MS with radioactivity detection, as described below.

Analytical Methods

Determination of Total Radioactivity

Total radioactivity in plasma, bile, urine and cage wash was determined in Insta-Gel® Plus (PerkinElmer, Waltham, MA) scintillation cocktail by liquid scintillation counting (LSC) on a Model 3100TR QuantaSmart Liquid Scintillation Counter (Packard Instrument Company, Meriden, CT). Total radioactivity in feces and blood was determined by LSC following sample combustion. Blood aliquots were accurately weighed in Combusto-Cones® containing Combusto-Pads® and burned in a Tri-Carb® Model 307 Sample Oxidizer (Packard). After mixing the combusted residue with 10 ml of Monophase® (Packard), total radioactivity was determined by LSC. Feces were sufficiently covered in 70 % ethanol in water, followed by homogenization with a high frequency homogenizer (Omni GLH-1, Omni International, Marietta, GA) prior to sample combustion.

Total radioactivity in tissue homogenates was determined by LSC following sample solubilization. Tissues except for bone were homogenized in 70 % ethanol in water. The exact weight of the homogenate was recorded. Duplicate aliquots of homogenate or bone were accurately weighed in scintillation vials in combination with a sufficient volume (approximately 0.5-2.0 ml) of 1N sodium hydroxide to digest the sample. Samples were placed in an incubator (model # 6DM, Thelco Lab, Precision Scientific, Winchester, VA) at approximately 40ºC overnight or until dissolved.

Following digestion, 10 ml of Insta-Gel® Plus scintillation cocktail was added and total radioactivity was determined by LSC.

Final radioactivity concentrations were determined from the specific activity of the dose solution using DEBRA data management software (Version 5.7.6.100, LabLogic Systems Ltd. Sheffield, UK).

Processing of Animal Samples for Metabolite Identification and Profiling

Rat plasma (90 µl) was pooled from three rats at each time point. Pooled samples were extracted with four volumes of acetonitrile/methanol (50/50, v/v), followed by vortexing and centrifugation at 3000 rpm at 4°C for 30 min using a Eppendorf 5810R centrifuge (rotor model: A4-81, Eppendorf AG, Hamburg, Germany). Supernatants were concentrated in a Savant SpeedVac (Thermo Fisher Scientific) for 4.5 h. The residue was reconstituted in 100 µl methanol/water (50/50, v/v) prior to HPLC-MS/MS analysis. Dog plasma (1-2 ml) at each time point was sequentially extracted with 5 and 8 ml of acetonitrile/methanol (50/50, v/v). Following vortexing and centrifugation, the supernatants were concentrated by SpeedVac overnight, and the residue was reconstituted in 180-240 µl methanol/water (50/50, v/v) prior to HPLC-MS/MS analysis.

Rat urine or bile samples were pooled at equal percent weight from each animal, followed by centrifugation. Supernatants were transferred to vials with inserts for HPLC-MS/MS analysis. Aliquots of individual dog urine and bile samples were filtered prior to HPLC-MS/MS analysis.

HPLC-MS/MS Analysis with Radioactivity Detection

Veliparib and its metabolites were identified and profiled in *in vitro* or *in vivo* studies following separation by HPLC and detection by an on-line or off-line radiochemical detector coupled with a mass spectrometer. HPLC system consisted of an Agilent 1100 Series binary pump and an Agilent 1100 series autosampler (Agilent Technologies, Santa Clara, CA). Elution of metabolites was achieved at room temperature on a Phenomenex Luna C18, 5 µm, 100 Å, 150 x 4.6 mm i.d. HPLC column (Phenomenex, Torrance, CA). The mobile phases consisted of 10 mM ammonium acetate in water at pH 4.0 (adjusted with acetic acid) (solvent A) and acetonitrile (solvent B). A gradient was applied consisting of 0 % B held for 10 min, followed by a linear gradient to 15 % B over the next 30 min before linear increase to 100 % B in 5 min. The gradient was held constant at 100 % B for 5 min before returning to initial condition of 0 % B in 1 min. The column was equilibrated at 0 % B for 9 min before next injection. The flow rate was maintained at 1.0 ml/min.

For on-line radioactivity detection (rat urine and bile, and dog urine), a flow scintillation detector equipped with a 500-µl liquid cell was used (IN/US β-Ram Model 5, Tampa, FL) with the scintillant (Flo-Scint™ III, PerkinElmer) flow of 2.4 ml/min. Data was processed using the Laura Light software (Version 4.0.5.130, LabLogic). For off-line radioactivity detection (rat plasma, dog bile and plasma), the HPLC effluent was collected into a 96-deep well LumaPlate (PerkinElmer) using a fraction collector (Model FC 204, Gilson, Inc, Middleton, WI) with a collection time of 3.0 s/well. The collected fractions were dried by SpeedVac, and then counted on a TopCount microplate scintillation counter (PerkinElmer). Radioactivity profiles were reconstituted by ProFSA software (Version 3.4.3.366, PerkinElmer).

Two MS instruments were used for metabolite characterization : 1) An LTQ-XL ion trap mass spectrometer (Thermo Fisher Scientific), equipped with an electrospray (ESI) source operated in the positive ionization mode, was used for metabolite identification of rat urine and bile, all dog samples and *in vitro* samples. Key MS operating/acquisition parameters were as follows: source voltage: 5 kV, capillary temperature: 275°C; capillary voltage: 25 V; tube lens offset: 135 V. 2) An LTQ-Orbitrap (Thermo Fisher Scientific), equipped with an ESI source operated in the positive ionization mode, was used for analysis of rat plasma, and to obtain high resolution mass for all metabolites with a resolution of 30,000. All measured metabolite masses were within ± 1 millimass unit of calculated masses for the proposed metabolite structures. Key MS operating/acquisition parameters were as follows: source voltage: 4 kV; capillary temperature: 350°C; capillary voltage: 47 V; tube lens offset: 35 V. The HPLC effluent was split with a ratio of 2:8 between the mass spectrometer and an on-line radioactivity detector or a fraction collector for off-line radioactivity detection.

Isolation of M3 from Dog Urine for NMR Analysis

From the 0 to 24 h urine collected from one dog, M3 was isolated using aforementioned HPLC system. The purified M3 was desalted on an Oasis HLB solid phase extraction cartridge (Waters, Milford, MA) and then dissolved in D_2O for NMR analysis. 1 D- and 2D-NMR experiments were conducted on a Varian Inova 500 MHz NMR spectrometer (Agilient Technologies) equipped with a SMIDG500 1.7 mm indirect detection gradient probe at Abbott Structure Chemistry Group (Abbott Park, IL).

Interactions of Veliparib with Human P-gp

Transport of Veliparib in MDR1-MDCKCells

Bidirectional permeability assay of veliparib (1 μM) was performed in both MDR1-MDCK and wild-type MDCK cell monolayers in triplicate. MDR1-MDCK and wild-type MDCK cells were grown to confluence for 5-10 days on 1 μm BD Falcon filters in 24-well plates. The donor solution contained 10 μM of veliparib in Hank's balanced salt solution (HBSS, pH 7.4) with 0.5 mg/ml of Lucifer Yellow and was supplemented with 25 mM HEPES (pH 7.4). The donor solutions were transferred to either the apical (Ap) or basolateral (Bl) chamber of the permeability diffusion apparatus. Receiver chambers contained 4 % bovine serum albumin in HBSS supplemented with 25 mM HEPES. Sequential samples of transported solute were taken at 20 min intervals using an automated liquid handling platform. The concentration of transported solute during each sampling interval was determined by HPLC-UV-MS (a Waters Alliance 2795 HPLC system coupled with a Waters Quattro Premier mass spectrometer, Waters). Permeability coefficients were calculated for each sampling interval using the following equation:

$$P_{app,i} = (V_D/A) *[(1/M_{D(0)})*(\Delta M_{R(t)} /\Delta t)]_{\ i^{th}\ interval}$$

Where V_D = volume of donor, A = surface area of the filter on which the monoplayer was grown (cm^2), $M_{D(0)}$ = mass in the donor at the beginning of t^{th} sampling interval, $\Delta M_{R(t)}$ = mass in the receiver at time t, and Δt is the experimental interval. The apparent permeability, P_{app}, is then calculated as the average:

$$P_{app} = (P_{app,1} + P_{app,2} + \ldots P_{app,\ n}) /n$$

Efflux ratio (ER) is defined as the ratio of apparent permeability between basolateral-to-apical and apical-to-basolateral directions. The net flux ratio is calculated as ratio of efflux ratio in MDR1-MDCK cells to efflux ratio in wildtype MDCK cells. Integrity of

cell monolayer was evaluated by measuring the amount of Lucifer Yellow in the receiver chambers at the end of the whole incubation period.

Inhibition of P-gp by Veliparib

The inhibition potential of veliparib (0-1000 μM) on the activity of human P-gp was evaluated in duplicate in the monolayer of Caco-2 cells (DKFZ, Heidelberg, Germany) using digoxin as the probe substrate. Caco-2 cells were grown on Transwell HTS polycarbonate filters (0.4 μm pore, 24-well format, Corning, NY) for 22 days prior to the experiment. For transport studies, cells were rinsed, pre-incubated in HBSS for 30 min, and further incubated for 60 min with HBSS containing the designated concentration of veliparib on both sides. Cell monolayers were then dosed with designated concentrations of veliparib and 10 μM of digoxin in HBSS containing 0.5 mg/ml of Lucifer yellow to either the apical or basolateral side of the filters. Aliquots were collected at 0 and 120 min from the donor side and at 30 and 120 min from the receiver side. Digoxin was extracted from the aliquots with cold ethanol containing ketoprofen as internal standard for positive ion mode and chloroxazone for negative ion mode. Extracted digoxin was quantitated by LC/MS/MS which consisted of an Agilent 1100 series HPLC system (Agilent Technologies) coupled with a AB Sciex 5000 mass spectrometry (AB Sciex, Foster City, CA). All procedures were done in a tissue culture incubator (Cytomat 2C450S, Thermo Fisher Scientific) maintained at 37°C with 5% CO_2. The Ap-to-Bl and Bl-to-Ap permeability (P_{app}) of digoxin and efflux ratios were calculated using the aforementioned methods.

RESULTS

***In Vitro* Metabolism** The *in vitro* metabolism of [^{3}H]veliparib was studied in various hepatic systems across species, including liver S9 fractions, liver microsomes and hepatocytes from mouse, rat, monkey, dog, and human . [^{3}H]Veliparib was stable (< 5 % metabolism) in all tested *in vitro* hepatic systems (data not shown). Using a panel of recombinant human CYP enzymes, metabolism of [^{3}H]veliparib was observed in incubations with CYP3A4, 2C19, 1A2, and 2D6*1 with turnover of 2.0, 3.4, 8.3, and 20.6%, respectively. Mono-oxygenation metabolite M2 was identified as the major metabolite and the lactam M8 was also detected in these incubations.

Structure Characterization of Veliparib Metabolites Structures of veliparib and its metabolites were elucidated by LC-MS/MS using a combination of full scan and product ion scans (MS^2 or MS^3) analyses of biological samples. The structure of M8 was supported by comparisons of its HPLC retention time and mass spectrum with those of a synthetic standard. M3 structure was characterized by 1D and 2D-NMR analysis. Structures of all other metabolites are proposed on the basis of high resolution mass and MS^2 fragmentation analysis.

Veliparib. Parent drug veliparib eluted at ~28 min on HPLC analysis, displaying a protonated molecular ion at *m/z* 245. MS/MS fragment ions at *m/z* 162 and 84 indicated the cleavage between benzoimidazole carboxamide and 2-methylpyrrolidine. The fragment ion at *m/z* 145 resulted from loss of NH_3 from the ion of *m/z* 162.

M1 and M2. Two metabolites (M1 and M2) with same protonated molecular ion of *m/z* 261 were observed in urine and plasma from rat and dog eluting at approximate 26 and

27 min, respectively, by HPLC analysis. High resolution MS analysis suggested addition of one oxygen atom (+ 16 amu) to veliparib. MS/MS analysis of M1 showed fragment ions at *m/z* 162 and 100, suggesting oxygenation on 2-methylpyrrolidine. MS/MS analysis of M2 produced fragment ions at *m/z* 178 and 84, suggesting that oxygenation occurred at the benzoimidazole carboxamide.

M3 and M4. M3 and M4 had the same protonated molecular ion at *m/z* 277, eluting at about 22 and 30 min by HPLC analysis of bile, plasma and urine from rat and dog, respectively. High resolution MS analysis suggested additions of two oxygen atoms (+ 32 amu) to veliparib. MS/MS analysis of M3 showed fragment ions at *m/z* 259 and 162, suggesting modification occurred at 2-methylpyrrolidine moiety. MS^3 analysis of ion *m/z* 259 gave fragment ions of *m/z* 242, 225, 162 and 145. The ion at *m/z* 225 resulted from loss of two NH_3 (-34 amu) from ion of *m/z* 259, suggesting that M3 was an amino acid metabolite. 1D-and 2D NMR analysis of M3 samples isolated from dog urine confirmed the proposed structure of amino acid. ^{1}H NMR (500 MHz, D_2O) δ 7.80 (d, J = 7.6 Hz, 1H), 7.75 (d, J = 8.0 Hz, 1H), 7.36 (t, J = 7.9 Hz, 1H), 2.31 – 2.24 (m, 2H), 2.05 (td, J = 7.3, 2.5 Hz, 2H), 1.73 (s, 3H). MS/MS analysis of M4 showed fragment ions at *m/z* 260, 259, 249, 232, 202 and 162. The presence of fragment ion at *m/z* 162 suggested that modification occurred at 2-methylpyrrolidine moiety.

M5 and M6. M5 was observed at about 19 min by HPLC analysis of bile from rat and dog and dog plasma, and M6 was observed at around 23 min only in rat bile. Both M5 and M6 had a protonated molecular ion of *m/z* 437. High resolution MS indicated additions of one oxygen atom (+16 amu) and a glucuronic acid (+176 amu) to afford a net gain of 192 amu as compared to veliparib. MS/MS fragmentation of M5 and M6

generated a common fragment ion of *m/z* 261, suggesting that M5 and M6 were formed through oxidation and glucuronidation of parent drug. MS/MS analysis of M5 produced a fragment ion of *m/z* 354, which resulted from cleavage of 2-methylpyrrolidine, indicating that modification occurred at benzoimidazole carboxamide. An additional ion of *m/z* 178 confirmed the modification site at benzoimidazole carboxamide. MS/MS analysis of M6 generated fragment ions of *m/z* 276 and 162, indicating that modification occurred at 2-methylpyrrolidine moiety.

M7 and M8. M7 and M8 eluted at around 33 and 37 min by HPLC analysis, respectively, displaying a protonated molecular ion at *m/z* 259. High resolution MS indicated addition of one oxygen atom (+16 amu) and loss of two hydrogens (-2 amu) compared to veliparib. MS/MS fragmentation of M7 resulted in fragment ions at *m/z* 242, 224, 214, 197, 162 and 145. The ions of *m/z* 162 and 145 suggested modification at 2-methylpyrrolidine. MS/MS fragmentation of M8 generated fragment ions at *m/z* 242, 162 and 98, indicating that M8 was formed from modification at 2-methylpyrrolidine. Lactam structure of M8 was confirmed by comparisons of HPLC retention time and MS spectrum with those of synthetic standard.

M9. M9 eluted at approximately 38 min by HPLC analysis of bile and plasma from rat and dog, showing a protonated molecular ion at *m/z* 465, 220 amu greater than molecular ion of veliparib. MS/MS analysis of M9 generated fragment ions at *m/z* 289, 245, 162 and 145, suggesting that M9 was a carbamoyl glucuronide with modification occurring at 2-methylpyrrolidine.

M10 and M11. Both M10 and M11 had a protonated molecular ion at *m/z* 451. M10 was only observed in rat bile with a HPLC retention time of around 27 min, and M11 was eluted at around 26 min during HPLC analysis of bile from both rat and dog. High resolution MS analysis suggested additions of two oxygen atoms (+32 amu) and a glucuronic acid (+176 amu) as well as loss of two hydrogens (-2 amu) to afford a net gain of 206 amu as compared to veliparib. MS/MS analysis of M10 showed fragment ions at *m/z* 275, 258, 162 and 145. The ions at *m/z* 162 and 145 indicated that modification occurred at the 2-methylpyrrolidine. The fragment ion of *m/z* 275 resulted from facile loss of a glucuronic acid (176 amu) and was 16 amu greater than molecular ion of M8, suggesting that M10 may be formed from M8 through sequential oxidation and glucuronidation at 2-methylpyrrolidine. MS/MS analysis of M11 showed fragment ions at *m/z* 434, 275, 258, 178 and 161. The ion at *m/z* 178 indicated that modification occurred at benzoimidazole carboxamide. The same fragment ion of *m/z* 275 suggested that M11 may be formed from M8 through sequential oxidation and glucuronidation at benzoimidazole carboxamide.

Mass spectrometric characterization of veliparib and its metabolites are shown in Table 1. The proposed biotransformation pathway of veliparib in rats and dogs is shown in Figure 2.

Absorption and Excretion of [^{3}H]Veliparib in Rats and Dogs Mean total recovery of radioactivity after 72 h was 95.7 % in rats and 91.3 % in dog for intravenous administration, and 97.6 % in rats and 84.3 % in dog for oral administration (Table 2). In both species, the dosed radioactivity was well absorbed and rapidly excreted in urine, with minimal radioactivity excreted in bile and feces. In rats given a 5 mg/kg intravenous

dose of [^{3}H]veliparib, mean total radioactivity recovery in 72 h was 79.4 % of dose in urine and < 5 % in bile or feces (Table 2). For oral administration, total dose recovery in 72 h was 82.7 % in urine, with 5.1 % of the dose recovered in bile, and 4.1 % in feces (Table 2). A nearly identical excretion profile was also observed in dogs following an intravenous or oral dose of 2.5 mg/kg (Table 2). Urinary elimination of radioactivity was rapid with greater than 70 % of the dose excreted within 24 h in both rats and dogs. Sum of radioactivity doses recovered in urine and bile from orally treated animals indicates that at least 87.8 % of dose was absorbed in rats and 75.9 % of the dose was absorbed in dog.

Metabolism of [^{3}H]Veliparib in Rats Veliparib was primarily excreted in rat urine as parent drug. Radioactivity profiles in the 0-24 h urine collected from intravenously dosed group showed that about 53.3 % of the dose was recovered as parent drug. In the 0-6 h bile, total radioactivity recovery was only 4.1 % of the dose, among which parent drug accounted for 0.6 % (Table 3). A total of ten metabolites (M1-M5, and M7-M11) were characterized in rat urine and bile. The most significant metabolite was the lactam M8, representing about 21.5 % of the dose (19.6 % in urine and 1.9 % in bile). Other metabolites were minor, each representing < 3 % of the dose (Table 3). Similar metabolism and elimination patterns were observed following a single 5 mg/kg oral dose of [^{3}H]veliparib to rats. Parent drug accounted for approximately 55.4 % of the dose in the 0-24 h urine and 0.6 % of the dose in the 0-6h bile. The major metabolite, M8, represented 23.7 % of the dose (21.5 % in urine and 2.2 % in bile). Other minor metabolites accounted for < 3 % of the dose (Table 3).

Following a 5 mg/kg intravenous dose of [^{3}H]veliparib to rats, parent drug was the most significant radiolabeled component in the circulation, representing 30.7-58.0 % of the total plasma radioactivity at 0.5, 1, 2 or 4 h postdose (Figure 3). M2 and M8 were two major metabolites in circulation, representing 13.8-28.8 % and 12.0-23.6 % of the total plasma radioactivity, respectively. M3, M4, M7 and M9 were identified as minor metabolites, with each representing < 10 % of total plasma radioactivity (Figure 3).

Metabolism of [^{3}H]Veliparib in Dogs Similar to rats, urine metabolite profile from intravenously dosed dog showed that about 44.0 % of the dose was excreted as unchanged parent drug within 24 h. Veliparib was not observed in dog bile. A total of ten metabolites (M1-M9 and M11) were identified. M3 and M8 were two significant metabolites in excreta, representing a total of 11.8 and 15.8 % of the dose, respectively (Table 3). The majority of M3 and M8 were excreted in urine, representing 11.3 % and 15.0 % of the dose, respectively. Other metabolites were minor, each accounting for less than 3 % of the dose. In circulation, parent drug was the major radiolabeled component at each sampling time point. Area under curve (AUC) of concentration-time profile within 0 and 8 h was estimated by using WinNonlin software (Version 4.0, Pharsight, Mountain View, CA). M2, M3 and M8 were identified as three major metabolites, with AUC_{0-8} values that were estimated to be 19.3, 21.3 and 28.8 % of veliparib AUC_{0-8}, respectively. Minor metabolites M4, M5, M7 and M9 were present, with each estimated AUC_{0-8} < 10 % of veliparib AUC_{0-8}.

Similar excretion and metabolism profiles were observed in orally treated dog. Within 24 h, approximately 41.1 % of the dose was recovered as parent drug in urine, with M3 and M8 accounting for additional 11.2 and 17.9 % of the dose, respectively (Table 3). In the

0-6 h bile, total radioactivity recovery was only 0.9 % and no parent drug was observed. Parent drug was the major radiolabeled component in dog plasma at each time point (Figure 4). M2, M3 and M8 were three major metabolites, with estimated AUC_{0-8} value representing 27.3, 38.5 and 47.8 % of parent AUC_{0-8}, respectively (Figure 4). Other metabolites M4, M5, M7 and M9 were minor (each < 10 % of parent AUC_{0-8}) (Figure 3).

Tissue Distribution of Radioactivity in Rats Following a 5 mg/kg intravenous dose of [^{3}H]veliparib to rats, the distribution of [^{3}H]veliparib was extensive with radioactivity quantifiable in all examined tissues. High tissue-to-plasma ratios (T:P) were observed in most of the tissues (T:P at 30 min postdose): kidney (5.3), liver (5.0), bone marrow (4.6), lungs (2.9), spleen (3.1), thymus (2.7), muscle (2.2), bone (1.6), skin (1.6), and heart (1.5), while lower T:P ratios were observed in testes (0.6), brain (0.3), while fat (0.3), and spinal cord (0.2) (supplemental Table 1). Highest maximum concentrations (ng equivalents [^{3}H]veliparib/g) were found in the kidneys (9537; 30 min), followed by liver (8966; 30 min), and bone marrow (8222; 30 min) (supplemental Table 1 and Figure 1). Maximum radioactivity concentrations were observed 30 min postdose in all tissues, and the concentrations declined with time. After 48 h postdose, less than 80 ng equivalents [^{3}H]veliparib/g of radioactivity remained in any of the selected tissues. T:P ratios generally decreased or remained unchanged for most tissues.

Interactions of Veliparib with Human P-gp Permeability and transport of veliparib were evaluated in triplicate in both MDR1-MDCK and wildtype MDCK cell monolayers at 1 μM to investigate if veliparib is a substrate for human P-gp (MDR1). Veliparib had high apparent apical-to-basolateral permeability values of $8.2 \pm 1.0 \times 10^{-6}$ cm/sec in wildtype MDCK cells and $13.4 \pm 2.1 \times 10^{-6}$ cm/sec in MDR1-MDCK cells. The efflux

ratio was 1.0 in wildtype MDCK cells and 1.8 in MDR1-MDCK cells. The net flux ratio of veliparib in MDR1-MDCK cells was calculated as 1.8, suggesting that veliparib was a weak substrate for human P-gp. Quinidine, ranitidine and talinolol are known P-gp substrates and were used as positive controls in the assay, showing the net flux ratio of 3.9, 2.9, and 10.7 in MDR1-MDCKcells, respectively. Recoveries of test articles were high (≥ 88%).

The inhibition potential of veliparib on the human P-gp activity was evaluated in Caco-2 monolayer using digoxin as the probe P-gp substrate at the veliparib concentrations of 0-100 μM in the first study and at 1000 μM in a second study. The efflux ratio of 9.2 for digoxin transport in Caco-2 cells was observed in the first study, and this efflux in digoxin transport was completely inhibited in the presence of the P-gp inhibitor verapmil at 30 μM (digoxin efflux ratio: 1.6). In contrast, veliparib did not demonstrate significant inhibition of the Pgp-dependent efflux of digoxin up to the highest tested concentration of 100 μM (digoxin efflux ratios: 7.5-14.7). In a second study, P-gp inhibition by veliparib was investigated in Caco-2 cells at the veliparib concentration of 1000 μM. An efflux ratio of 4.2 was observed for digoxin transport, which was inhibited by 30 μM of verapmil (digoxin efflux ratio: 1.4), but not affected by 1000 μM of veliparib (digoxin efflux ratio: 4.9).

DISCUSSION

Veliparib, a novel PARP inhibitor being developed for treatment of cancers, demonstrated high and rapid absorption. In bile duct-cannulated rats and dogs, at least 87.8 % and 75.9 % of dosed radioactivity were absorbed, respectively, consistent with high oral bioavailability (> 60 %) (Donawho et al., 2007). Similarly in human, high absorption of veliparib was indicated by, on average, 70 % of dose being recovered as parent drug in urine (Kummar et al., 2009). Veliparib absorption was also rapid with T_{max} ranging from 0.5 to 2.3 h in animals and 0.5-1.5 h in humans after oral administration (Donawho et al., 2007; Kummar et al., 2009).

Renal secretion is the primary route of veliparib clearance. In bile duct-cannulated rats and dogs, drug-related materials were primarily eliminated in urine, with a significant portion as parent drug (> 40 % of dose). Consistently in human, about 70 % of dose was excreted in urine as parent drug. An *in vitro* study demonstrated that veliparib is a substrate for human organic cation transporter 2 (OCT2), a renal transporter involved in active secretion of cationic drugs (manuscript in preparation). Both *in vivo* excretion profiles and *in vitro* transporter data suggest the involvement of active renal secretion and support the conclusion that renal clearance is the primary mechanism of veliparib clearance. The excretion profile of veliparib is similar to that of varenicline, which is also primarily excreted as parent drug in urine of animals and humans, and is an OCT2 substrate (Obach et al., 2006; Feng et al., 2008). In a clinical DDI study with cimetidine, an OCT2 inhibitor, a small increase in varenicline exposure was observed (Feng et al., 2008). It was also indicated that moderate increase of varenicline exposure was observed in patients with renal impairment (Obach et al., 2006). Given the similarity of clearance

mechanisms between veliparib and varenicline, veliparib exposure could be altered with concomitantly administered cimetidine or in patients with renal impairment. The clinical significance of these potential interactions may need further evaluation.

Metabolism plays a secondary role in veliparib clearance. In excreta of animals, metabolites contributed up to 33 % the dose. A total of 11 metabolites were characterized. The lactam M8 was the most significant metabolite in both species, accounting for 15-24 % the dose. The amino acid metabolite M3 represented approximately additional 11 % of the dose in dogs. In circulation, M8 and mono-oxygenated metabolite M2 were two major metabolites in rats and dogs. M3 was another major circulatory metabolite in dogs. Consistent with animal plasma profiles, M8 was a major plasma metabolite in patients receiving veliparib (Wiegand et al., 2010). M8 was about 5 fold less potent than veliparib for *in vitro* PARP inhibition (K_i: 23 nM) (Penning et al., 2009). A radiolabeled mass balance study has not been conducted in humans and radioactivity profiles of human plasma and urine are unknown. Metabolite profiling studies with non-radiolabeled human plasma samples suggested that the preliminary metabolite profile was similar to those in rats and dogs. Parent drug was the major component and three metabolites were characterized including M8 as a major metabolite, and two minor metabolites: M2 and M9 (*N*-carbamoyl glucuronide) (unpublished data).

Veliparib metabolism mainly occurred on the pyrrolidine to generate lactam, amino acid, *N*-carbamoyl glucuronide, as well as products of mono-oxygenation, and oxidation followed by dehydrogenation. Additional mono-oxygenation occurred on the benzoimidazole carboxamide. Other secondary glucuronide metabolites were formed from above primary metabolites. Pyrrolidine is well known to be metabolized to form

lactam *via* either iminium ions or carbinolamines (Vickers and Polsky, 2000). The amino acid metabolite is not believed to be formed from lactam hydrolysis; rather it is proposed to arise from the amino aldehydes that may be produced from ring opening of unstable carbinolamine intermediates (Vickers and Polsky, 2000). Multiple recombinant human CYPs including CYP2D6, 1A2, 2C19 and 3A4 demonstrated the ability to metabolize veliparib to generate M2 and M8.

Veliparib demonstrated wide tissue distribution and crossed blood-brain barrier (BBB) in rats. Following a single intravenous dose of [^{3}H]veliparib to rat, the dosed radioactivity distributed widely to all selected tissues, consistent with high volume of distribution (3.1 L/kg) observed in rat pharmacokinetics profile. Highest radioactivity concentrations were observed in kidneys, consistent with the predominant urinary excretion of drug-related radioactivity. Drug-related radioactivity was observed in brain with brain to plasma radioactivity concentration ratio (B:P) ranging from 0.3 to 1, indicating moderate brain penetration. The data is consistent with previous results for central nervous system (CNS) penetration in mouse, rat and monkey, in which veliparib demonstrated B:P of approximately 1:3 in rats and mice, and cerebrospinal fluid penetration of about 57% in monkey (Donawho et al., 2007; Penning et al., 2009; Muscal et al., 2010). Since human P-gp in BBB is primarily responsibly for limiting the entry of drugs into brain, it is important to characterize whether veliparib is a substrate for human P-gp. A previous study reported a good B:P of 0.98 in wildtype mice treated with a single intravenous dose of 10 mg/kg of veliparib. B:P increased in *mdr1a/1b* double knockout (KO) (4.5), *bcrp* KO (1.5) or triple KO mice (7.5), indicating that brain penetration of veliparib was affected by P-gp and BCRP (Fan et al., 2010). Consistently in our study,

veliparib was shown to be a weak substrate for P-gp with a low net flux ratio of 1.8 in MDR1-MDCK cells. A net flux ratio over 2 is considered a positive result for P-gp substrate (FDA, 2006). Although veliparib is a weak substrate for P-gp and its brain penetration was affected by P-gp, due to its high permeability, veliparib could still penetrate through the BBB *via* passive diffusion to achieve sufficient exposure. This result would be consistent with the finding that veliparib in combination with TMZ demonstrated efficacy in a preclinical brain tumor model (Donawho et al., 2007). Veliparib is being investigated in clinical trials in patients with brain and CNS tumors (clinicaltrials.gov).

P-gp has also been reported to cause clinically significant DDIs *via* P-gp inhibition or induction, i.e. digoxin-verapamil and digoxin-rifampicin (Marchetti et al., 2007). A number of anti-cancer chemotherapeutics such as paclitaxel, doxorubicin, and topotecan are known P-gp substrates, and are being co-administered with veliparib. To further characterize the potential DDIs of veliparib with these P-gp substrates, we evaluated whether veliparib inhibits P-gp activity using digoxin as a probe substrate in Caco-2 cells. Our study demonstrated that veliparib did not inhibit P-gp-mediated digoxin transport up to 1000 μM. The projected clinically efficacious dose of veliparib in combination of TMZ is 40 mg twice a day. The intestinal concentration of veliparib is estimated to be about 650 μM, at which veliparib is not expected to inhibit P-gp activity in the intestine. A good *in vitro-in vivo* correlation was established for varenciline. Varenciline did not have clinically relevant effect on digoxin exposure *in vivo*, supported by *in vitro* studies that varenicline was neither a P-gp substrate nor an inhibitor of P-gp

mediated efflux of digoxin in Caco-2 cells (Faessel et al., 2008). Overall, veliparib would not be expected to have clinically significant P-gp-mediated DDIs.

In addition, veliparib is not likely to cause clinically significant DDIs mediated by CYPs. Veliparib was metabolized *in vitro* by multiple recombinant human CYPs including CYP1A2, 2D6*1, 2C19 and 3A4. The highest turnover was observed with CYP2D6*1, consistent with a previous study, in which CYP2D6 was shown to be the predominant enzyme for veliparib metabolism (Li et al., 2009). Common allelic variants CYP2D*10 and * 4 showed reduced catalytic activities, as compared to wildtype CYP2D6, indicating that CYP2D6 pharmacogenetics may affect veliparib pharmacokinetics and efficacy in clinical studies (Li et al., 2009). CYP2D6 polymorphism has been associated with clinically relevant DDIs when drugs significantly rely on the enzyme either for clearance or metabolism to an active metabolite (de Groot et al., 2009). However, in humans, 70% of veliparib dose, on average, was excreted in urine as parent, thus, metabolism contributed to at most 30 % of total clearance. In addition, veliparib was metabolized by multiple pathways including oxidation catalyzed by others CYPs and UGT-mediated *N*-carbamoyl glucuronidation. Contribution of CYP2D6 to total veliparib clearance may not be significant in humans. Therefore, CYP2D6 polymorphism or co-administration of veliparib with CYP2D6 inhibitors would not cause clinically significant DDIs. In addition, veliparib didn't inhibit activities of CYP1A2, 2A6, 2C9, 2C19, 2D6, 2E1, 2B6, 2C8 and 3A4 in human liver microsomes (IC_{50} > 30 μM), and induce the activities of CYP1A2, 2B6, 2C9 and 3A4 in human hepatocytes up to 10 μM (data not shown). Those concentrations obtained in *in vitro*

evaluations are much greater than projected efficacious plasma concentration of 0.78 μM in clinics.

In summary, veliparib disposition was characterized by high absorption, wide tissue distribution, and primary renal clearance followed by metabolic clearance. In urine and plasma, the major drug-related component was unchanged veliparib. Veliparib is not likely to cause clinically relevant DDIs mediated by P-gp and CYPs. Altogether, these attributes point to favorable dispositional and DDI profiles, the desirable characteristics for a safe and effective therapeutic agent.

Acknowledgements

The authors would like to thank Dr. Bruce Surber for synthesis of [^{3}H]veliparib, David Whittern for conducting NMR experiments. We acknowledge Mark Mason, Robin Shapiro, and Tanita Mason-Bright for conducting animal studies. We also thank Drs. Daniel Bow, Alexander Shoemaker, and Vincent Giranda for their support and critical review of the manuscript.

Authorship Contributions:

Participated in research design: Delzer and Lao

Conducted experiments: Li, Delzer and Lao

Performed data analysis: Li, Delzer and Lao

Wrote or contributed to the writing of the manuscript: Delzer, Voorman, de Morais and Lao

REFERENCES

American Cancer Society (2010) Cancer facts & figures 2010, American Cancer Society, Atlanta, GA USA.

De Groot MJ, Wakenhut F, Whitlock G, and Hyland R (2009) Understanding CYP2D6 interactions. *Drug Discov Today* **14**: 964-972.

Donawho CK, Luo Y, Luo Y, Penning TD, Bauch JL, Bouska JJ, Bontcheva-Diaz VD, Cox BF, DeWeese TL, Dillehay LE, Ferguson DC, Ghoreishi-Haack NS, Grimm DR, Guan R, Han EK, Holley-Shanks RR, Hristov B, Idler KB, Jarvis K, Johnson EF, Kleiberg LR, Klinghofer V, Lasko LM, Liu X, Marsh KC, McGonigal TP, Meulbroek JA, Olson AM, Palma JP, Rodriguez LE, Shi Y,Stavropoulos JA, Tsurutani AC, Zhu GD, Rosenberg SH, Giranda VL, and Frost DJ (2007) ABT-888, an orally active poly(ADP-ribose) polymerase inhibitor that potentiates DNA-damaging agents in preclinical tumor models. *Clin Cancer Res* **13**: 2728-2737.

Faessel HM, Burstein AH, Troutman MD, Willavize SA, Rohrbacher KD, and Clark DJ (2008) Lack of a pharmacokinetic interaction between a new smoking cession theapy, varenicline, and digoxin in adult smokers. *Eur J Clin Pharmacol* 64: 1101-1109.

Fan L, de Gooijer MC, Beumer JH, Christner SM, Beijnen JH, and van Tellingen O (2010) ABC transporters in the blood-brain barrier limit the brain penetration of the

PARP inhibitor ABT-888. *AACR Annual Meeting, Washington DC, USA* **101**: Abs LB-49.

FDA (2006) Guidance for industry: drug interaction studies-study design, data analysis, and implications for dosing and labeling, FDA, Rockville, MD USA.

Feng B, Obach RS, Burstein AH, Clark DJ, de Morais SM and Faessel HM (2008) Effect of human renal cationic transporter inhibition on the pharmacokinetics of varenicline, a new therapy for smoking cessation: an *in vitro-in vivo* study. *Clin Pharmacol Ther* **83**: 567-576.

Kummar S, Kinders R, Guitierrez ME, Rubinstein L, Parchment RE, Phillips LR, Ji J, Monks A, Low JA, Chen A, Murgo AJ, Collins J, Steinberg SM, Eliopoulos H, Giranda VL, Gordon G, Helman L, Wiltrout R, Tomaszewski JE, and Doroshow JH (2009) Phase 0 clinical trial of the poly(ADP-ribose) polymerase inhibitor ABT-888 in patients with advanced malignancies. *J Clic Oncol* **27**: 2705-2711.

Li J, Sha X, LoRusso P (2009) Pharmacogenetics of a PARP inhibitor ABT-888 metabolic pathway. *J. Clin Oncol* **27** (suppl; abstr e14556)

Marchetti S, Mazzanti R, Beijnen JH, and Schellens JHM (2007) Concise review: clinical relevance of drug-drug and herb-drug interactions mediated by the ABC transporter ABCB1 (MDR1, P-glycoprotein). *The Oncologist* **12**: 927-941.

Molina JR, Northfelt DW, Erlichman C, Lensing JL, Luo Y, and Giranda V (2009) Ongoing Phase 1 studies of a novel PARP inhibitor, ABT-888: pharmacokinetics, safety and anti-tumor activity. *AACR Annual Meeting, Denver, CO, USA* **100**: Abs 3602.

Muscal JA, Thompson PA, Giranda VL, Dayton BD, Bauch J, Horton T, McGuffey L, Nuchtern JG, Dauser RC, Gibson BW, Blaney SM, and Su JM (2010) Plasma and cerebrospinal fluid pharmacokinetics of ABT-888 after oral administration in non-human primates. *Cancer Chemother Pharmacol* **65**: 419-425.

Obach RS, Reed-Hagen AE, Krueger SS, Obach BJ, O'Connell TN, Zandi KS, Miller S, and Coe JW (2006) Metabolism and disposition of varenicline, a selective $\alpha_4\beta_2$ acetylcholine receptor partial agonist, in vivo and in vitro. *Drug Metab Dispos* **34**: 121-130.

Palma JP, Wang YC, Rodriguez LE, Montgomery D, Ellis PA, Bukofzer G, Niquette A, Liu X, Shi Y, Lasko L, Zhu GD, Penning TD, Giranda VL, Rosenberg SH, Frost DJ, and Donawho CK (2009) ABT-888 confers broad in vivo activity in combination with temozolomide in diverse tumors. *Clin Cancer Res* **15**: 7277-7290.

Papeo G, Forte B, Orsini P, Perrera C, Posteri H, Scolaro A, and Montagnoli A (2009) Poly (ADP-ribose) polymerase inhibition in cancer therapy: are we close to maturity? *Expert Opin. Ther. Patents* **19**: 1377-1400.

Penning TD, Zhu GD, Gandhi VB, Gong J, Liu X, Shi Y, Klinghofer V, Johnson EF, Donawho CK, Frost DJ, Bontcheva-Diaz VD, Bouska JJ, Osterling, DJ, Olson AM, Marsh KC, Luo Y, and Giranda VL (2009) Discovery of the poly(ADP-ribose) polymerase (PARP) inhibitor 2-[(*R*)-2methylpyrrolidin-2-yl]-1*H*-benzimidazole-4-carboxamide (ABT-888) for the treatment of cancer. *J Med Chem* **52**: 514-523.

Penning TD (2010) Small-molecule PARP modulators-current status and future therapeutic potential. *Curr Opin Drug Discov Devel* **13**: 577-586.

Rouleau M, Patel A, Hendzel MJ, Kaufman SH, and Poirier GG (2010) PARP inhibition: PARP1 and beyond. *Nature Review Cancer* **10**: 293-301.

Vickers S, and Polsky SL (2000) The biotransformation of nitrogen containing xenobiotics to lactams. *Curr Drug Metab* **1**: 357-389.

Wiegand R, Wu J, Sha X, LoRusso P, and Li J (2010) Simultaneous determination of ABT-888, a poly (ADP-ribose) polymerase inhibitor, and its metabolite in human plasma by liquid chromatography/tandem mss spectrometry. *J Chromatogr. B* **878**: 333-339.

Xu J, Kochanek, K. D., Murphy, S., and Tejada-Vera, B (2010) Deaths: final data for 2007. *National Vital Statistics Reports* **58**, Centers for Disease Control and Prevention, Atlanta, GA USA.

FOOTNOTE

This work was previously presented as follows: Voorman R, Li X, Shoemaker A, Penning T, Giranda V, Delzer J, de Morais S, and Lao Y (2010) Veliparib (ABT-888), a novel, potent PARP inhibitor with favorable ADME properties. *International ISSX Meeting, Istanbul, Turkey* **9**: Abs: P142.

DMD Fast Forward. Published on March 24, 2011 as DOI: 10.1124/dmd.110.037820
This article has not been copyedited and formatted. The final version may differ from this version.

FIGURE LEGEND

Figure 1. Structure of [^{3}H]veliparib: T denotes site of tritium labeling

Figure 2. Proposed biotransformation pathway of veliparib in rats and dogs

Figure 3. Representative plasma HPLC-radiochromatograms from rat (0.5 hr) receiving a 5 mg/kg intravenous dose and dog (6 hr) receiving a 2.5 mg/kg oral dose of [^{3}H]veliparib

Figure 4. Plasma concentration-time profiles of total radioactivity, unchanged veliparib and major metabolites M2, M3 and M8 after a single oral administration of 2.5 mg/kg [^{3}H]veliparib to a dog

Table 1. Mass spectrometric characterization of veliparib and its metabolites in plasma, bile or urine from rats and dogs

ID	$[M+H^+]$	Proposed Formula	Fragment Ions (*m/z*)	Biotransformation	Matrix
veliparib	245	$C_{13}H_{16}N_4O$	MS^2: 84, 145, 162		bile, urine, plasma (R, D)
M1	261	$C_{13}H_{16}N_4O_2$	MS^2: 100, 162, 216	mono-oxidation	urine (R, D), plasma (D)
M2	261	$C_{13}H_{16}N_4O_2$	MS^2: 84, 178, 216	mono-oxidation	urine, plasma (R, D)
M3	277	$C_{13}H_{16}N_4O_3$	MS^2: 162, 259 MS^3 of *m/z* 259: 98, 145, 162, 242	pyrrolidine ring-opening	bile, urine, plasma (R, D)
M4	277	$C_{13}H_{16}N_4O_3$	MS^2: 162, 202, 232, 249, 259, 260	di-oxidation or pyrrolidine ring-opening	bile, urine, plasma (R, D)
M5	437	$C_{19}H_{24}N_4O_8$	MS^2: 161, 178, 261, 337, 354	oxidation + glucuronidation	bile (R, D), plasma (D)
M6	437	$C_{19}H_{24}N_4O_8$	MS^2: 145, 162, 209, 226,	oxidation + glucuronidation	bile (R)
M7	259	$C_{13}H_{14}N_4O_2$	MS^2: 98, 145, 162, 197, 214, 224, 242	oxidation + dehydrogenation	bile, urine, plasma (R, D)
M8	259	$C_{13}H_{14}N_4O_2$	MS^2: 98, 162, 242	lactam formation	bile, urine, plasma (R, D)
M9	465	$C_{20}H_{24}N_4O_9$	MS^2: 145, 162, 245, 289	carbamoyl glucuronidation	bile, plasma (R, D)
M10	451	$C_{19}H_{22}N_4O_9$	MS^2: 145, 162, 258, 275	M8 + oxidation + glucuronidation	bile (R)
M11	451	$C_{19}H_{22}N_4O_9$	MS^2: 161, 178, 258, 275, 434	M8 + oxidation + glucuronidation	bile (R, D)

R: rat; D: dog

Table 2. Cumulative recovery of radioactivity (expressed as % of dose) in urine, feces, cage wash and bile after a 5 mg/kg i.v. or oral dose to BDC rats and a 2.5 mg/kg i.v. or oral dose to BDC dogs

Animal	Route	Dose (mg/kg)	Animal (N)	Recovery of Radioactivity (% dose)					
				Timepoint (h)	Urine	Bile	Feces	Cage Wash	Total Recovery
Rats	i.v.	5	3	0-24	78.4 ± 7.0	4.5 ± 0.7	3.0 ± 1.2	ns	85.9 ± 5.1
				0-72	79.3 ± 6.3	4.7 ± 0.7	3.7 ± 1.0	8.0 ± 3.1	95.7 ± 2.1
	oral	5	3	0-24	82.0 ± 8.8	4.9 ± 1.2	3.7 ± 1.0	ns	90.6 ± 6.6
				0-72	82.7 ± 8.4	5.1 ± 1.2	4.1 ± 1.1	5.7 ± 5.0	97.6 ± 1.2
Dogs	i.v.	2.5	1	0-24	76.7	2.4	0.9	0.9	80.9
				0-72	83.7	2.4	3.8	1.4	91.3
	oral	2.5	1	0-24	71.8	1.9	4.1	2.7	80.5
				0-72	74	1.9	4.9	3.5	84.3

i.v.: intravenous; BDC: bile duct-cannulation; ns: no sample

Rat data were presented as mean ± SD.

Table 3: Distribution of veliparib and its metabolites in urine and bile from rats and dogs (expressed as % of dose)

Animal (dose)	Rat (5 mg/kg)				Dog (2.5 mg/kg)			
Matrix	Urine		Bile		Urine		Bile	
Dosing Route	i.v.	oral	i.v.	oral	i.v.	oral	i.v.	oral
Timepoint (h)	0-24	0-24	0-6	0-6	0-24	0-24	0-6	0-6
M1	nd	nd	nd	nd	1.5	0.7	nd	nd
M2	nd	nd	nd	nd	2.2	1.2	nd	nd
M3	1.6	1.7	0.5	0.3	**11.3**	**11.2**	0.5	0.3
M4	2.4	2.5	0.1	0.1	1.5	0.8	ms	ms
M5	nd	nd	0.4	0.4	nd	nd	0.2	0.1
M6	nd	nd	nd	nd	nd	nd	0.1	0.1
M7	2.4	1.7	0.04	nd	1.2	1.2	ms	ms
M8	**19.6**	**21.5**	1.9	2.2	**15.0**	**17.9**	0.8	0.3
M9	nd	nd	0.5	0.9	nd	nd	0.2	0.04
M10	nd	nd	0.1	0.1	nd	nd	nd	nd
M11	nd	nd	0.1	0.1	nd	nd	nd	nd
Veliparib	53.3	55.4	0.6	0.6	44	41.1	nd	nd
Others [a]	nd	nd	nd	nd	nd	nd	0.2	0.1
Total Recovery [b]	78.4	82.7	4.1	4.6	76.7	74.0	0.1	0.9

nd: not detected; i.v.: intravenous dose; ms – detected by MS; bold type indicates major excretory metabolites.

[a.] Unidentified components

[b.] Total dose recovery is calculated from sum of all quantifiable metabolites.

DMD Fast Forward. Published on March 24, 2011 as DOI: 10.1124/dmd.110.037820
This article has not been copyedited and formatted. The final version may differ from this version.

Figure 1

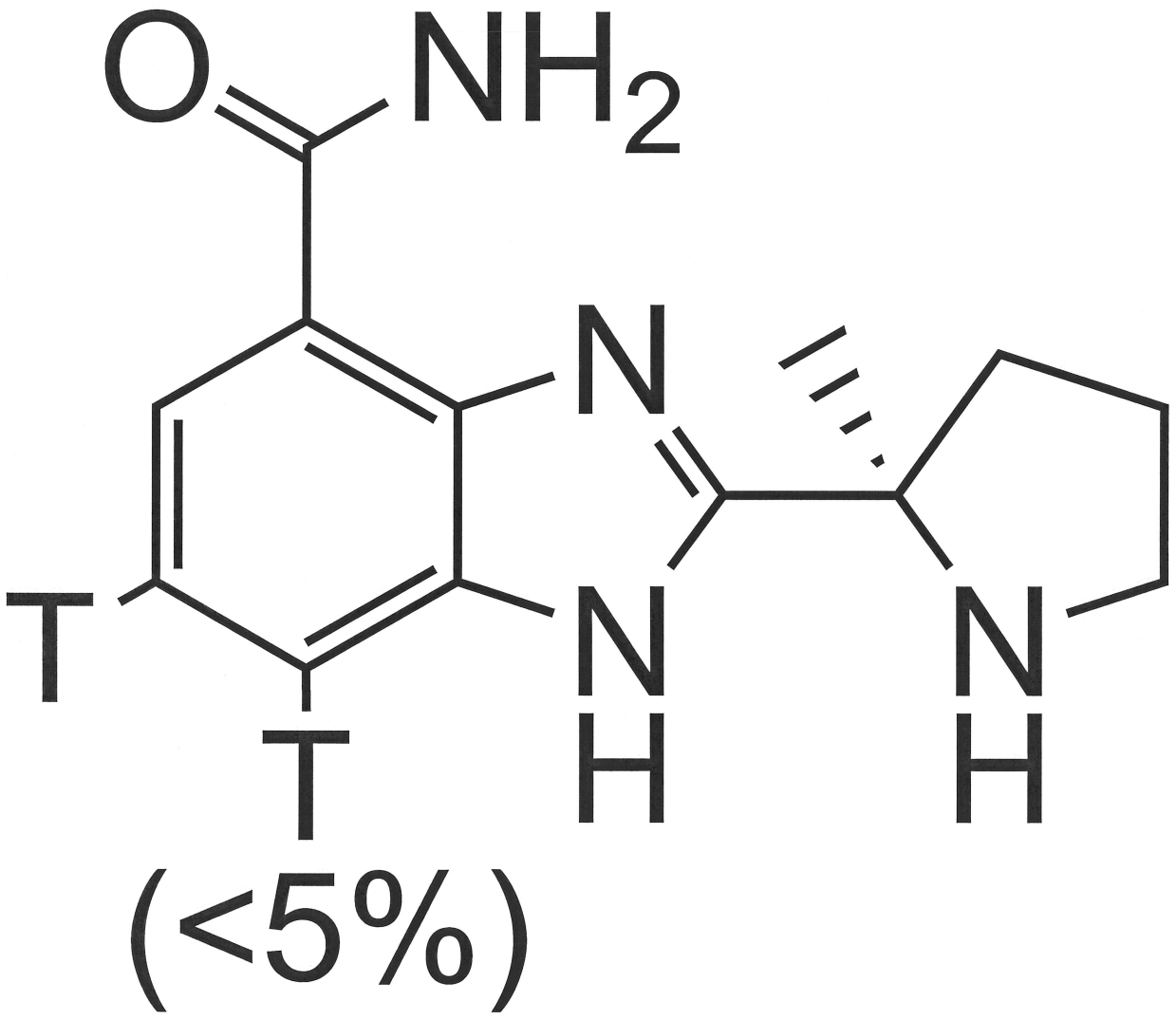

Figure 2

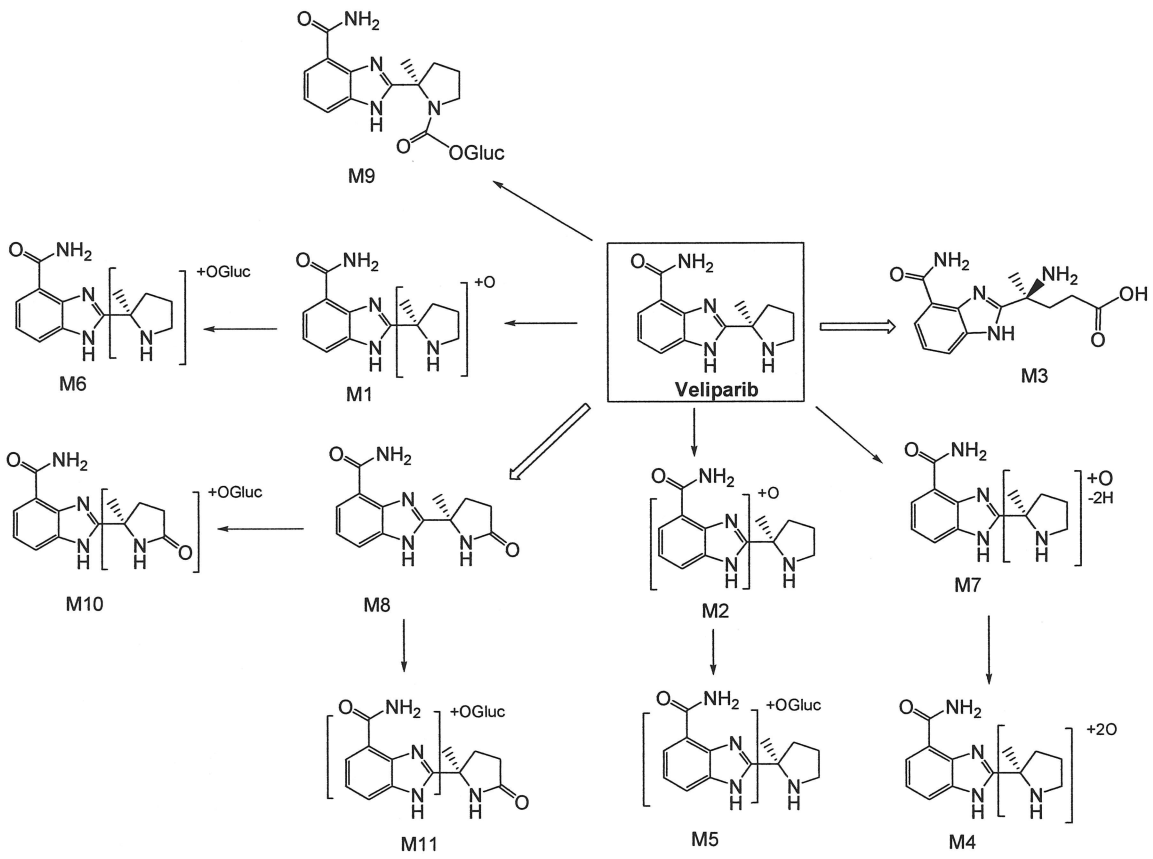

Figure 3

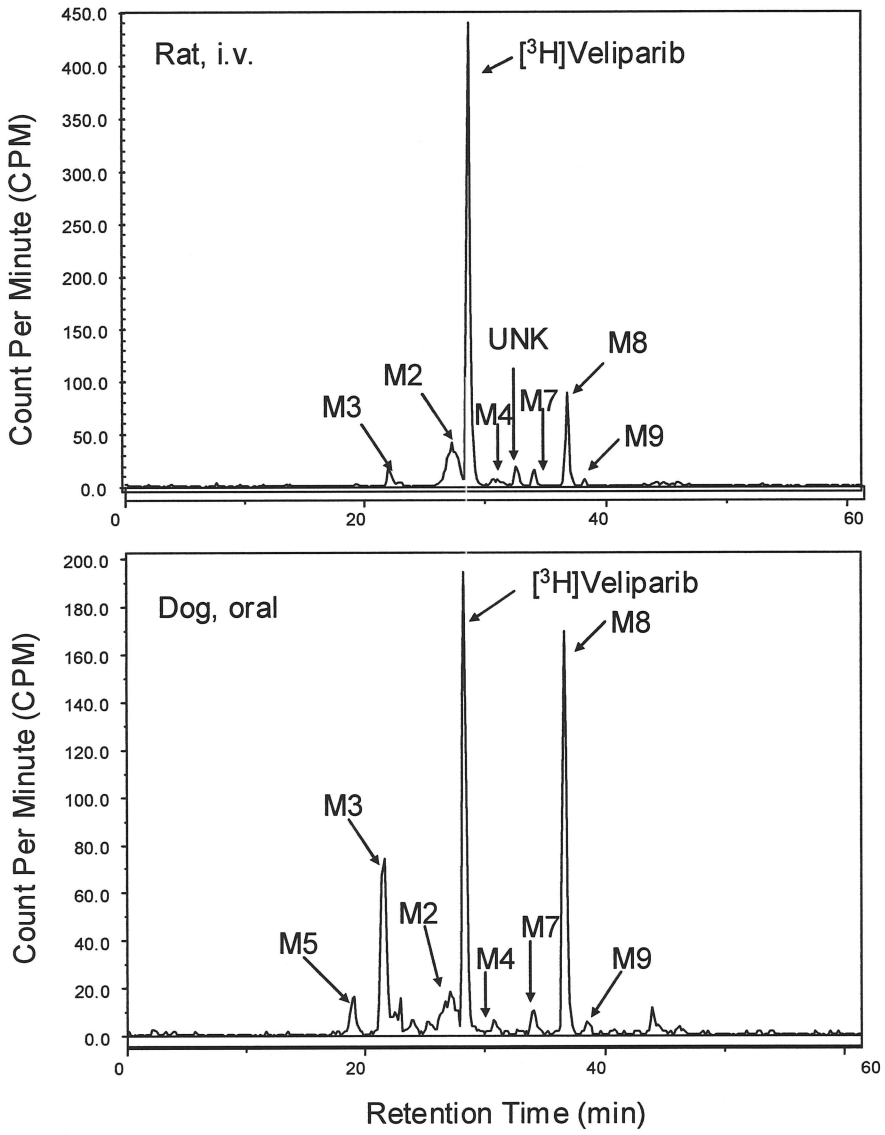

Figure 4

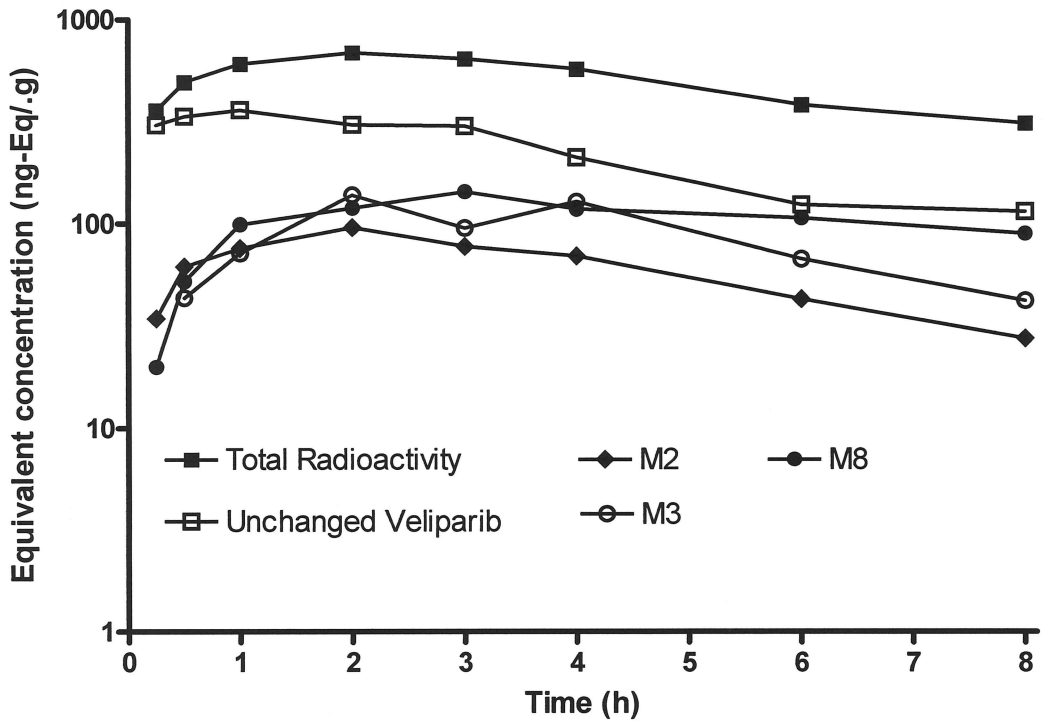

SUPPLEMENTAL DATA

Title: DISPOSITION AND DRUG-DRUG INTERACTION POTENTIAL OF VELIPARIB (ABT-888), A NOVEL AND POTENT INHIBITOR OF POLY(ADP-RIBOSE) POLYMERASE

Authors: Xiaofeng Li, Juergen Delzer, Richard Voorman, Sonia M. de Morais, and Yanbin Lao

Journal: Drug Metabolism & Disposition

Legend for Supplemental Table

Supplemental Table 1. Radioactivity concentrations (ng equivalent of [^{3}H]veliparib/g) and tissue-to-plasma concentration ratios (T:P) following a single 5 mg/kg intravenous dose of [^{3}H]veliparib to rats (N=2). Data are presented as mean of two rats

Legend for Supplemental Figure

Supplemental Figure 1. Radioactivity concentration-time profiles in selected tissues (kidneys, liver, bone marrow, blood and plasma) after a single intravenous administration of 5 mg/kg [^{3}H]veliparib to rats (N=2). Data are presented as mean of two rats

Supplemental Table 1. Radioactivity concentrations (ng equivalent of [^{3}H]veliparib/g) and tissue-to-plasma concentration ratios (T:P) following a single 5 mg/kg intravenous dose of [^{3}H]veliparib to rats (N=2). Data are presented as mean of two rats

Tissues	0.5h		1h		2h		4h		6h		24h		48h	
	Concentration (ng/g)	T:P	Concentration (ng/g)	T:P	Concentration (ng/g)	T:P	Concentration (ng/g)	T:P	Concentration (ng/g)	T:P	Concentration (ng/g)	T:P	Concentration (ng/g)	T:P
Blood	1971	1.1	1254	1	973	1.1	372	1	188	1	65	1	55	1.2
Brain	496	0.3	413	0.3	290	0.3	108	0.3	112	0.6	58	0.9	48	1
Eyes	1793	1	1193	1	786	0.9	321	0.9	214	1.2	85	1.3	44	0.9
Bone Marrow	8222	4.6	4553	3.7	2819	3.2	1080	3	469	2.6	94	1.4	39	0.8
Bone	2844	1.6	1435	1.2	810	0.9	347	1	227	1.2	49	0.7	28	0.8
Heart	2780	1.5	1779	1.5	1253	1.4	547	1.5	287	1.6	48	1	48	1
Kidneys	9537	5.3	6370	5.2	4461	5	2210	6.2	1618	8	88	1.3	76	1.6
Liver	8966	5	5121	4.2	3719	4.1	1319	3.7	675	3.7	100	1.5	77	1.6
Lungs	5277	2.9	2984	2.5	2105	2.3	649	1.8	364	2	69	1	51	1.1
Muscles	3954	2.2	3605	3	2160	2.4	699	1.9	301	1.7	79	1.2	41	0.9
Plasma	1801	1	1216	1	900	1	358	1	182	1	67	1	47	1
Skin	2921	1.6	2552	2.1	1759	1.9	629	1.8	295	1.6	90	1.3	59	1.2
Spinal cord	333	0.2	314	0.3	223	0.2	119	0.3	114	0.6	48	0.7	41	0.9
Spleen	5599	3.1	3261	2.7	2050	2.3	621	1.7	517	2.7	79	1.2	58	1.2
Testes	1049	0.6	1108	0.9	1169	1.3	934	2.6	565	3.2	117	1.8	75	1.6
Thymus	4792	2.7	3116	2.6	1970	2.2	771	2.2	326	1.8	78	1.2	55	1.2
White fat	582	0.3	404	0.3	293	0.3	132	0.4	123	0.6	13	0.2	9	0.2

Supplemental Figure 1